Mesoscale Numerical Study over the HEIFE Area. Part 1: Three Dimensional Wind Field

AUTHOR(S):

CHEN, Zhong; CHEN, Jiayi; MITSUTA, Yasushi; ISHIKAWA, Hirohiko

CITATION:

CHEN, Zhong ...[et al]. Mesoscale Numerical Study over the HEIFE Area. Part 1: Three Dimensional Wind Field. Bulletin of the Disaster Prevention Research Institute 1996, 45(2-3): 39-60

ISSUE DATE:

1996-02

URL:

http://hdl.handle.net/2433/125009

Bull. Disas. Prev. Res. Inst., Kyoto Univ., Vol. 45, Part 2,3 No. 390, February, 1996

Mesoscale Numerical Study over the HEIFE Area Part 1: Three Dimensional Wind Field

By Zhong CHEN[1], Jiayi CHEN[1], Yasushi MITSUTA and Hirohiko ISHIKAWA

(Manuscript received on Oct. 23, 1995, revised on Feb. 9, 1996)

Abstract

In this study the three dimensional mesoscale model, which is based on the Peking University Mesoscale Model, was used to simulate the wind field in the HEIFE experimental region. Simulations were conducted for two separate cases, one for strong synoptic flow and the other for thermally driven local circulation in weak synoptic flow. In the former case, the channeling effect caused by topographic constraint was significant and the computed wind followed the topographic feature. In the latter case, development of the local circulation was successfully reproduced by the model. The results were compared with meteorological data obtained in HEIFE. The agreement of computed and analyzed fields were discussed.

1. Introduction

The Heihe River Basin Field Experiment (HEIFE) is a Sino-Japanese cooperative research program focusing on the interaction processes between atmosphere and land surface in Gansu Province in northwestern China. The orography and the surface characteristics in this area are extremely complicated. The highest plateau in the world, Qinghai-Tibetan Plateau, is located southwest of the site. North of the HEIFE area is the Mongolian desert which is one of the major global dust sources. The HEIFE experimental area and its surrounding area have a variety of land surface characteristics, such as Gobi (rock desert), desert, cultivated land, wilderness, forests, meadows and glaciers.

One of the major objectives of HEIFE is to obtain aerial knowledge of land surface-atmosphere interaction over the semi-arid area. Although intensive observation has been carried out during the HEIFE project and various quantities including sensible and latent heat flux from land surface to the atmosphere were directly measured, another research step is needed to integrate the observed data to aerial information over the HEIFE area.

As for the meteorological factors such as wind, temperature and specific humidity, numerical simulation can be an effective tool in investigating their spatial distribution and temporal evolution, since it can produce three dimensional fields with these variables in a dynamically consistent way. In this study the Peking University

1) Visiting scientists from Department of Geophysics, Peking University

Mesoscale Model (Sang et al., 1992) was used to simulate the structure and evolution of wind, temperature, and humidity field in the HEIFE region. The model is a three dimensional hydrostatic meso-scale model and is formulated in the terrain following coordinates. Atmospheric turbulence is predicted by the turbulent closure scheme developed by Arritt (1987) on the basis of Yamada (1983). The surface processes are parameterized by the NP-89 model developed by Noilhan and Planton (1989). Sang et al. (1992) used the model to study the thermal and moisture modifications for two-dimensional flow between Gobi and oasis. The present study extends the former study to a three dimensional flow over complex terrain.

The model is described in the next section. The computational conditions are described in section 3. The predicted wind field for two typical cases, one representing prevalent synoptic flow, and the other, the well-developed local circulation, are shown and compared with diagnostic wind field and surface wind data at individual sites in section 4.

This paper is the first report of our study. Particular attention is paid to the wind field, since it is of principal importance in the atmospheric transport of various quantities. It has already been shown that there are significant spatial and temporal variations in this area by Tang (1963), Inoue and Mitsuta (1990), Chen et al. (1993) and Sahashi et al. (1993). The thermal structure, moisture transport and energy budget will be discussed in Part 2 of this paper.

2. Model Equations

The model is formulated in the terrain following coordinates, $(x, y, \bar{z})$. $\bar{z}$ is defined as

$$\bar{z}=H\frac{Z-Z_g}{H-Z_g}, \tag{1}$$

where Z_g is the ground elevation and H a reference height. With hydrostatic approximation the equations for mean quantities are written as,

$$\frac{\partial u}{\partial t}=-u\frac{\partial u}{\partial x}-v\frac{\partial u}{\partial y}-\bar{w}\frac{\partial u}{\partial \bar{z}}-\theta\frac{\partial \pi}{\partial x}+g\frac{\bar{z}-H}{H}\frac{\partial Z_g}{\partial x}+fv+D_u, \tag{2}$$

$$\frac{\partial v}{\partial t}=-u\frac{\partial v}{\partial x}-v\frac{\partial v}{\partial y}-\bar{w}\frac{\partial v}{\partial \bar{z}}-\theta\frac{\partial \pi}{\partial y}+g\frac{\bar{z}-H}{H}\frac{\partial Z_g}{\partial y}-fu+D_v, \tag{3}$$

$$\frac{\partial \pi}{\partial \bar{z}}=-\frac{g}{\theta}\frac{H-Z_g}{H}, \tag{4}$$

$$\frac{\partial u}{\partial x}+\frac{\partial v}{\partial y}+\frac{\partial \bar{w}}{\partial \bar{z}}-\frac{u}{H-Z_g}\frac{\partial Z_g}{\partial x}-\frac{v}{H-Z_g}\frac{\partial Z_g}{\partial y}=0, \tag{5}$$

$$\frac{\partial \theta}{\partial t}=-u\frac{\partial \theta}{\partial x}-v\frac{\partial \theta}{\partial y}-\bar{w}\frac{\partial \theta}{\partial \bar{z}}+D_\theta, \tag{6}$$

$$\frac{\partial q}{\partial t}=-u\frac{\partial q}{\partial x}-v\frac{\partial q}{\partial y}-\bar{w}\frac{\partial q}{\partial \bar{z}}+D_q, \tag{7}$$

where $(u, v, \bar{w})$ are the velocity components in the $(x, y, \bar{z})$ coordinates, θ potential temperature, q specific humidity and π the Exner function. The vertical velocity in the

terrain following coordinates, $\bar{w}$, relates with u, v, and w as

$$\bar{w}=w\frac{H}{H-Z_g}+u\frac{\bar{z}-H}{H-Z_g}\frac{\partial Z_g}{\partial x}+v\frac{\bar{z}-H}{H-Z_g}\frac{\partial Z_g}{\partial y}. \tag{8}$$

The D_ϕ ($\phi=u$, v, θ *and* q) are diffusion terms for u, v, θ and q, expressed as

$$D_\phi=K_H\left(\frac{\partial^2\phi}{\partial x^2}+\frac{\partial^2\phi}{\partial y^2}\right)+\left(\frac{H}{H-Z_g}\right)^2\frac{\partial}{\partial\bar{z}}\left(K_z\frac{\partial\phi}{\partial\bar{z}}\right), \tag{9}$$

where K_H and K_z are horizontal and vertical diffusion coefficients, respectively. The equations (2) and (3) are a couple of horizontal momentum equations and Eq. (4) the hydrostatic relation. Equations (5), (6) and (7) are conservation equations for mass, heat and water vapor, respectively.

In order to incorporate the surface effect properly, the vertical exchange coefficients in Eq. (9), K_z for u and v and K_θ for θ and q, are computed using a first-order turbulence parameterization by Arritt (1987). In the model, the turbulent kinetic energy, $e=(u'^2+v'^2+w'^2)/2$, is predicted by a formula by Yamada (1983),

$$\frac{de}{dt}=\frac{H}{H-Z_g}K_z\left[\left(\frac{\partial u}{\partial\bar{z}}\right)^2+\left(\frac{\partial v}{\partial\bar{z}}\right)^2\right]-K_\theta\frac{g}{\theta}\frac{\partial\theta}{\partial\bar{z}}+\frac{H}{H-Z_g}\frac{\partial e}{\partial\bar{z}}-\frac{(2e)^{2/3}}{B_1 l}+D_e, \tag{10}$$

where D_e is the diffusion term as in Eq. (9). The diagnostic length scale is defined as

$$l=S_m^{1/2}l_n, \tag{11}$$

where l_n is the length scale under neutral stability and is defined by Blackadar (1962) as

$$l_n=\frac{k\bar{z}}{1+k\bar{z}/l_\infty}. \tag{12}$$

In Eq. (12), k is the von Karman constant. Equation (12) specifies l_n as essentially being equal to kz near the ground, consistent with the surface-layer similarity theory. At greater heights, $l_n\to l_\infty$. The asymptotic length scale was specified as $l_\infty=100$ m following Louis (1979). The stability factor, S_m, in Eq. (11) is a function of the flux Richardson number as given by Yamada (1983). With the known turbulent kinetic energy and the length scale, the exchange coefficients are computed by

$$K_z=l(2e)^{1/2}S_m, \tag{13}$$

$$K_\theta=\alpha K_m, \tag{14}$$

$$K_e=(2e)^{1/2}lS_q. \tag{15}$$

The inverse turbulent Prandtl number, α is a function of the flux Richardson number, and S_q is an empirical constant in Yamada (1983). At the bottom layer, e is computed by the formula given by Louis (1979) in the same way as Arritt (1987).

At the bottom boundary the soil-vegetation-atmosphere model developed by Noilhan and Planton (1989) is used. The model is hereafter abbreviated as NP89 model. The NP89 model consists of the following partial differential equations:

$$\frac{\partial T_s}{\partial t}=C_T(R_n-H-LE)-\frac{2\pi}{\tau}(T_s-T_2), \tag{16}$$

$$\frac{\partial T_2}{\partial t}=\frac{1}{\tau}(T_s-T_2), \tag{17}$$

$$\frac{\partial W_g}{\partial t}=\frac{C_1}{\rho_w d_1}(P_g-E_g)-\frac{C_2}{\tau}(W_g-W_{geq}), \tag{18}$$

$$\frac{\partial W_2}{\partial t}=\frac{1}{\rho_w d_2}(P_g-E_g-E_{tr}), \tag{19}$$

$$\frac{\partial W_r}{\partial t}=VegP-E_r. \tag{20}$$

Here, T_s is the soil surface temperature, T_2 the diurnal average temperature down to about 1 m, W_g the volumetric soil moisture at the top 1 cm (d_1), W_2 the diurnal average volumetric soil moisture down to about 1 m (d_2), and W_r the amount of water in the vegetation canopy. P is the precipitation rate and P_g is the precipitation rate reaching the ground. E_g, E_{tr}, and E_r are the evaporation rate from the ground, evaporation rate due to transpiration, and evaporation rates from wet parts of canopy, respectively. These are calculated by

$$E_g=(1-Veg)\rho_a C_H V_a(h_u q_{sat}(T_s)-q_s), \tag{21}$$

$$E_r=Veg\rho_a\frac{\sigma}{R_a}(q_{sat}(T_s)-q_s), \tag{22}$$

$$E_{tr}=Veg\rho_a\frac{1-\sigma}{R_a+R_s}(q_{sat}(T_s)-q_a), \tag{23}$$

where h_u is the relative humidity at the ground parameterized as

$$h_u=\begin{cases}\frac{1}{2}\left[1-\cos\left(\frac{W_g}{W_{fc}}\pi\right)\right] & for\ W_g<W_{fc}\\ 1 & for\ W_g>W_{fc}\end{cases}. \tag{24}$$

Veg is the fractional vegetation coverage, and σ is the wet fraction of the canopy. The surface resistance for evapotranspiration is computed as

$$R_s=\frac{R_{smin}}{LAI\,F_1F_2F_3F_4}, \tag{25}$$

where leaf area index (*LAI*) and the minimum stomatal resistance R_{smin} are specified according to land-use classification. R_a is aerodynamic resistance. The fractional conductance F_1, F_2, F_3, and F_4 are functions of solar radiation, root-level soil moisture W_2, air humidity deficit, and ambient air temperature, respectively. The functional form of these conductances are seen in Noilhan and Planton (1989) and Jacquemin and Noilhan (1990). It should be noted that the soil moisture (W_g and W_2) are limited by the soil saturation point (W_{sat}). Similarly, W_r is limited by a maximum value $(W_r)_{\max}$ depending upon the density of the canopy. According to Dickinson (1984), we use the simple equation $(W_r)_{\max}=0.2\times Veg\ LAI$ [mm].

Equation (16) shows that local change of soil surface temperature results from the residual of the surface energy balance among net radiation R_n, surface sensible heat flux H, latent heat flux LE, and soil heat flux parameterized as a restoring force on the soil temperature back toward the diurnal average (τ is the time constant—1 day). C_t is the inverse of the bulk heat capacity of the surface and vegetation, which is the function of the deeper layer soil moisture W_2 (Noilhan and Planton, 1989). The C_1, C_2 and W_{geq} are

expressed in terms of soil parameters, such as field capacity, wilting point, saturation point, and various thermal and hydraulic properties of soil. The expression of these are found in the appendix of Jacquemin and Noilhan (1990).

R_n is calculated from parameterized long-wave and short-wave radiation components (Pielke, 1984). The surface momentum flux and the sensible heat flux, H are determined from wind speed, surface roughness and temperature difference between the surface and the lowest atmospheric layer by the bulk aerodynamic method suggested by Louis (1979). The latent heat flux, LE is the sum of the following three components of evaporation: transpiration E_{tr}, evaporation from wet part of the canopy E_r, and the direct evaporation from the ground surface E_g. The surface roughness is assumed as 0.03 m over desert and Gobi, 0.3 m over oasis and 1.0 m over mountainous region. The actual roughness height over the flat desert site is about 0.002 m but 0.03 m was used considering the slight undulation within the 5 km grid.

In applying the NP89 model to the HEIFE area, the surface characteristics are read from a land-use map of the area. The values of the parameters used in this paper are based on Sang et al. (1992), which are close to the original NP89, but with slight adjustment.

The finite difference forms of the above equations are constructed and are solved numerically. The staggered grid is used. The Donner Scheme is used to compute advection terms. The centered difference is used for the diffusion terms. The leap-frog is used for time integration. The time step is 10 seconds.

3. Application to Heihe River Basin

The Heihe River Basin is in the Hexi Corridor in the northwest China. Fig. 1(a) is a map of the area around the basin, in which topography is sketched by heavy contours. This region is one of major pathways of weather systems developing in and west of Xinjiang Autonomous Region. Due to the topographic features, the dominant wind is expected to be northwesterly or southeasterly when the region is under the influence of active synoptic disturbances. When the synoptic wind is weak, on the other hand, local circulation will develop which is driven by thermal contrasts of various causes such as mountain-valley or desert-oasis, and of various scales. Chen et al. (1993) classified the wind pattern in the basin into 'synoptic flow' and 'local flow'. According to their classification, the model is applied to two cases representing both categories. Hereafter, the simulation of the strong synoptic flow case is referred to as *Case 1* and the other as *Case 2*.

In the application of the model, two different computational domains are used, which are shown in Fig. 1(a) by rectangles. The smaller one covers a horizontal range of 60 km × 120 km, which is used in *Case 1*. The larger domain covers an area of 120 km × 170 km, which is used in *Case 2*. Figs. 1(b) and (c) are three dimensional views of the larger domain seen from different directions. The Heihe river flows in the middle of the computational domain from SE to NW. Thus, the SE edge of the domain is generally higher than the NW edge at the bottom of the basin. The SW edge of the domain is

bounded by Qilian Mountains, and the NE edge by lower mountains called LongShou Mountain and Heli Mountain.

The horizontal grid interval is set as $\Delta x = \Delta y = 5$ km. Thus, the smaller and the larger computational area are divided to 12×14 and 24×34 horizontal grids, respectively. In the vertical, grids are placed at 0, 10, 80, 150, 250, 350, 500, 750, 1000, 1250, 1750, 2000, 2500, 3000, 4000, 5000, 6000, 8000, and 10000 m above surface.

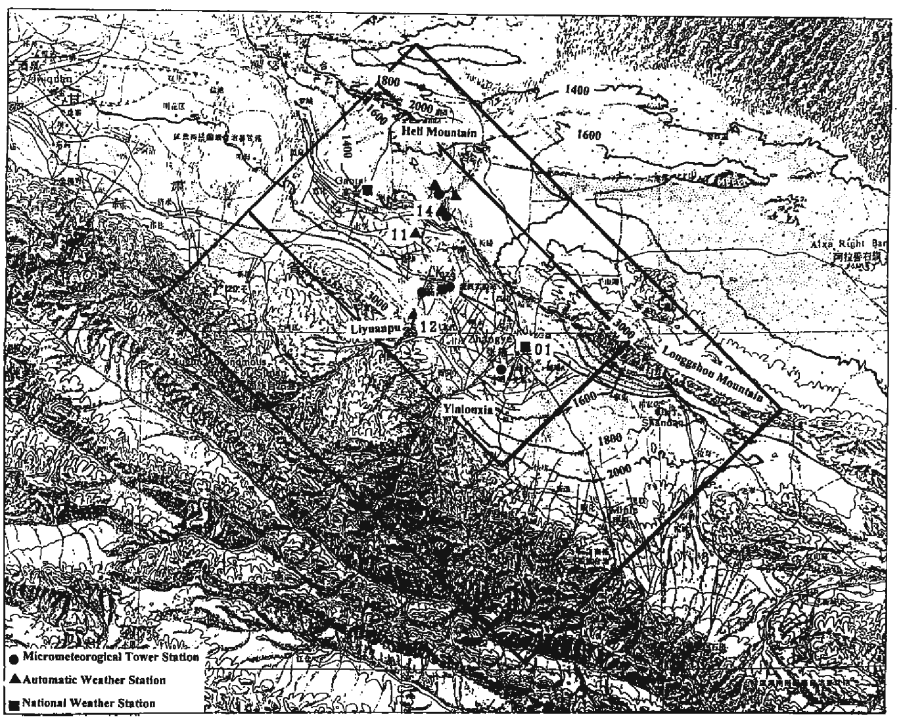

Fig. 1(a). The map of the HEIFE experimental area and simulation domain.

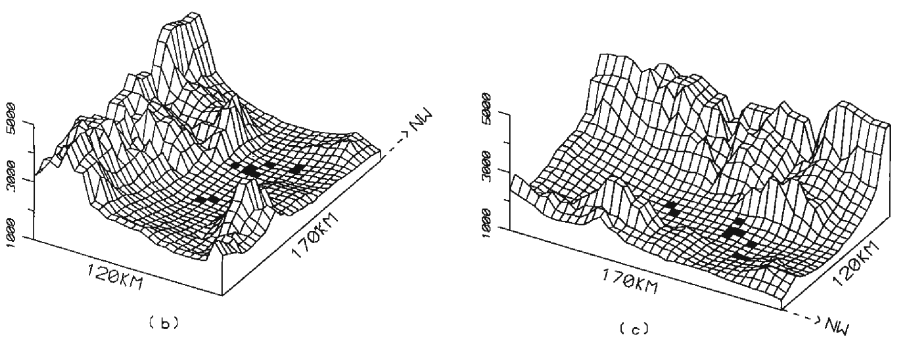

Fig. 1(b), (c). The three dimensional view of the terrain of the larger simulation domain seen from the east and north. The black squares in (b) and (c) indicate main observation points.

The constant inflow and gradient outflow condition are adopted at the lateral boundaries. At the top boundary, five absorbing layers are placed to damp the gravity wave. At the bottom boundary, $u=v=\bar{w}=0$ is used. The surface temperature and moisture are computed by the NP89 model.

The meteorological data used in the simulation come from eight HEIFE surface stations, three surface stations of the Chinese Meteorological Administration (CMA), and one aerological station of CMA, Zhangye. The HEIFE stations provide hourly data, the CMA surface stations at 3-hour intervals, and CMA aerological stations twice daily soundings.

4. Results

4. 1 *Case 1*; August 10, 1991, synoptic flow

There had been a low pressure on the surface extending from north of Qinghai-Tibet towards the northeast since Aug. 6, 1991. On Aug. 9, a cold front was approaching the experimental region and the easterly wind became stronger both at the surface and 700 hPa level. According to weather reports and observation records, the cold front passed the HEIFE area on Aug. 10. At the surface and the lower troposphere, the wind direction turned northwesterly at 0800 BST (Beijing Standard Time), and the wind speed increased. The change of surface wind field analyzed by a MASCON model (Chen et al., 1993) is shown in Fig. 2.

The simulation started at 0800 BST. The initial meteorological field from the bottom up to 2000 m above surface was set up using the result of the MASCON model (Fig. 2), in which available meteorological data were interpolated to each computational grid and the wind field was adjusted to satisfy mass-conservation. Above 2000 m, the initial values are assumed to be the same as those at the 2000 m level. At the inflow boundary, the results from hourly analysis by the MASCON model was used as the boundary value. Here, the boundary values above 2000 m were assumed to be the same as that of 2000 m, too. At the outflow boundary, the gradient outflow condition was used. The initial vertical profile of potential temperature is given by,

$$\theta=\begin{cases}300 & (z\leq 2000\ \mathrm{m})\\ 300+0.5*\dfrac{z-2000}{100} & (z>2000\ \mathrm{m})\end{cases}$$

This is also used as the boundary value at the inflow boundary. The computation of specific humidity was not performed in *Case 1*, since it has less importance in simulating the wind field in the strong wind condition.

The respective simulated surface wind fields at 1100, 1400, 1700 and 2000 BST are given in Fig. 3. Strong northwesterlies prevailed over the domain during the simulation period. The simulated wind flow fairly follows the topography of the corridor. The wind speed is relatively low over Zhangye oasis. This is partly because the width of the corridor expands there. The other reason is the larger surface roughness, and hence a greater surface drag exists over the oasis.

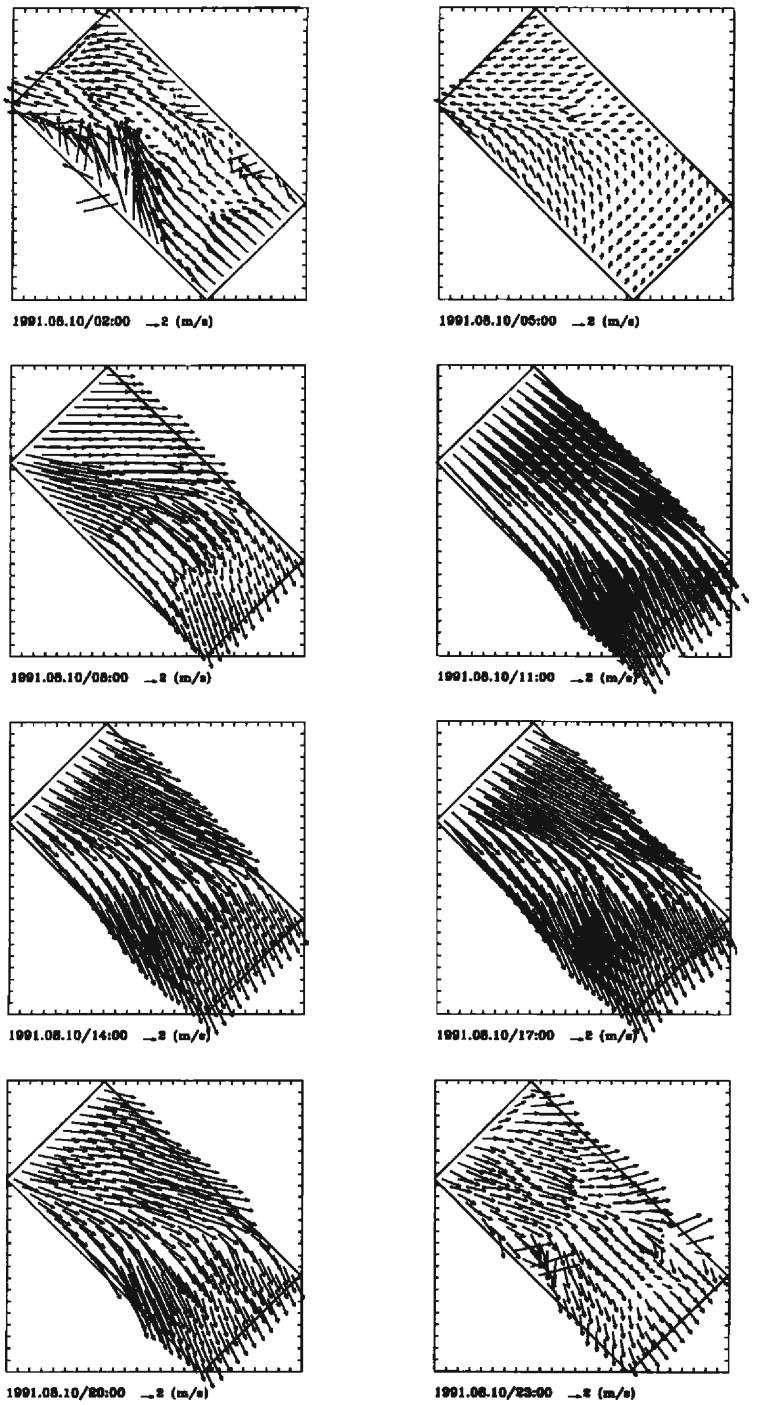

Fig. 2. Diagnostic results of surface wind field (10 m) at tri-hourly intervals on August 10, 1991.

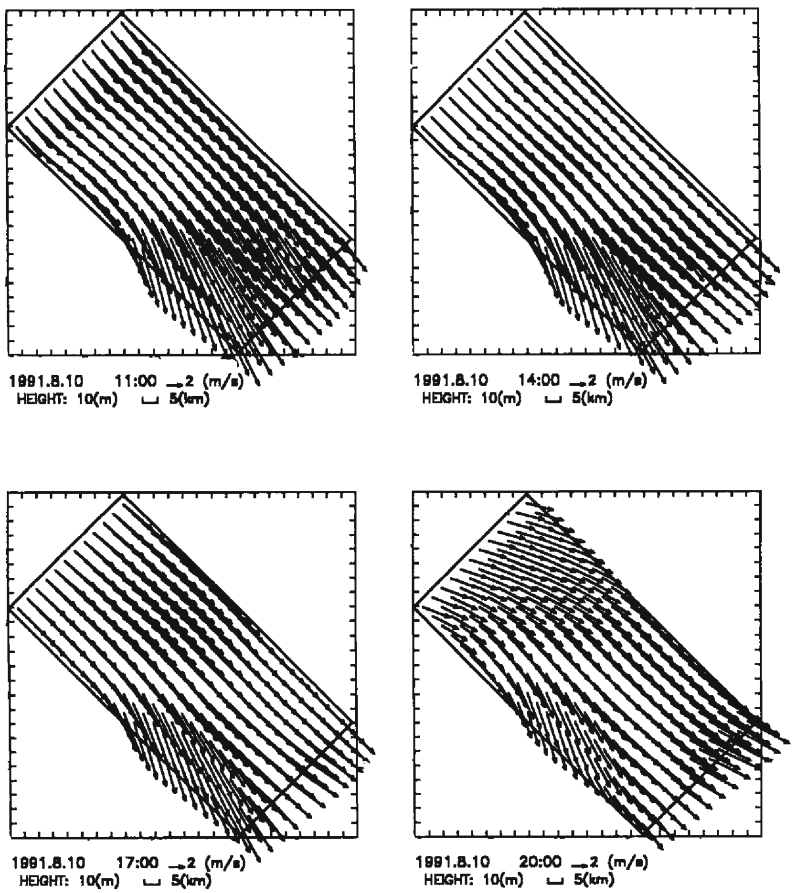

Fig. 3. Simulation results of surface wind field (10 m) at 1100, 1400, 1700 and 2000 BST (Beijing Standard Time) on August 10, 1991.

The simulated surface wind is compared with the observed wind in Fig. 4 for the four surface stations. Generally, the wind direction is well-simulated. However, the reproduction of the wind velocity is conditional. Especially at 2000BST, the model underestimates the wind velocity at site 12 and 14.

4. 2 *Case 2*; August 10, 1991, Local flow

On this day a weak low pressure was located in Hexi Corridor, and the wind speed was generally low. Although there were cirrus and scattered cumulus in the sky, the incoming solar radiation was strong during the daytime. So, it was in rather good conditions for the occurrence of thermally driven local circulation. Chen et al. (1993) analyzed the wind field of the day by a diagnostic model using data collected by HEIFE observational network, which are shown in Fig. 5.

The simulation by the model started at 2000 BST. The initial condition was

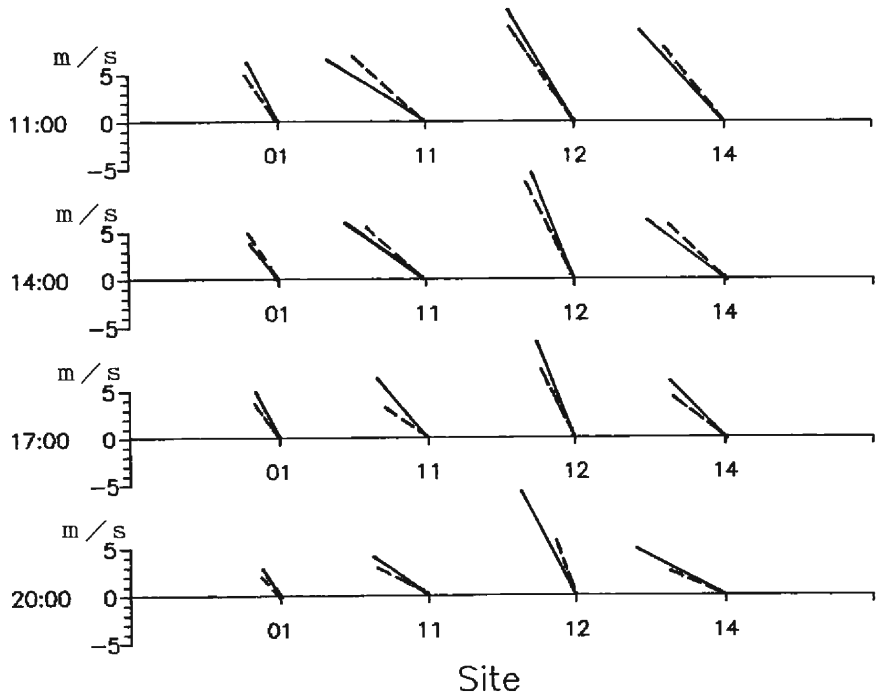

Fig. 4. Comparison of simulated and observed wind at some surface stations. The solid line represents observed wind direction and wind velocity and the broken line represents simulated wind direction and velocity.

$$u(x, y, \bar{z})=v(x, y, \bar{z})=\bar{w}(x, y, \bar{z})=0$$
$$q=q_0 e^{-z/300} \qquad (q_0=6.3 \text{ for oasis, } q_0=4.1 \text{ for desert or Gobi}).$$

The initial value of the potential temperature was the same as in *Case 1*. To adjust the model to the initial condition, the model ran without surface forcing for the first six hours, thereafter surface forcing was exerted.

The simulated wind field near the surface (10 m above surface) is shown in Fig. 6(a). It is seen that the flow field consists of two different spatial scales. The flow of the larger spatial scale follows the Heihe river basin itself; northwesterly in the daytime and southeasterly at night. At the side slopes of the corridor, a smaller scale flow, upslope in daytime and downslope in nighttime, is seen.

At 0500 BST, downslope winds were predominant everywhere. At 1100 BST, upslope winds started at the foot of the mountain, but the downslope flow still existed at the Qilian Mountains southwest of the computational domain. In the northwest, where there are low mountains, the downslope flow had stopped. At 1400 BST, upslope flow was dominant everywhere. At 2300 BST, downslope winds were dominant again everywhere. The transition from the nighttime flow regime to the daytime flow regime occurred at around 1100 BST. The reverse transition occurred at about 2000 BST. In

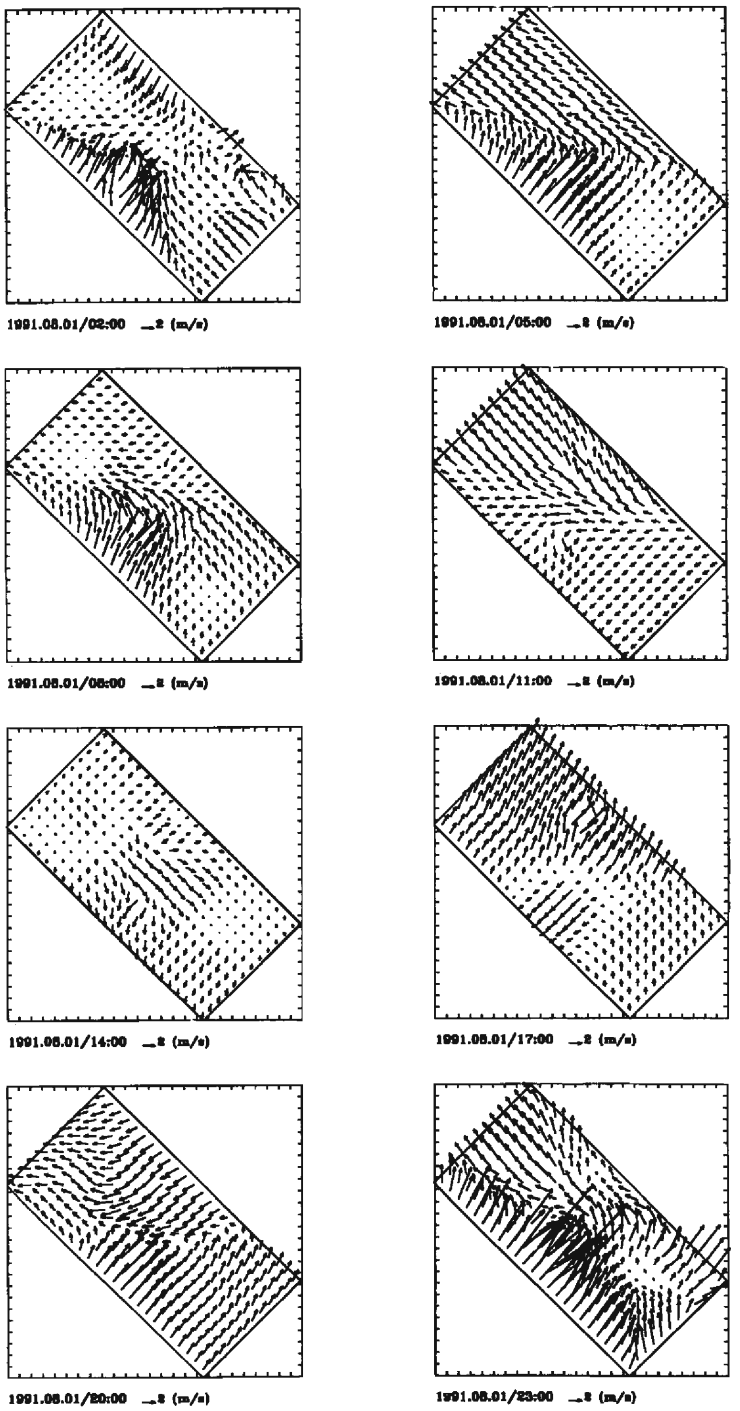

Fig. 5. Diagnostic results of local wind field at 10 m at tri-hourly intervals on August 1, 1991.

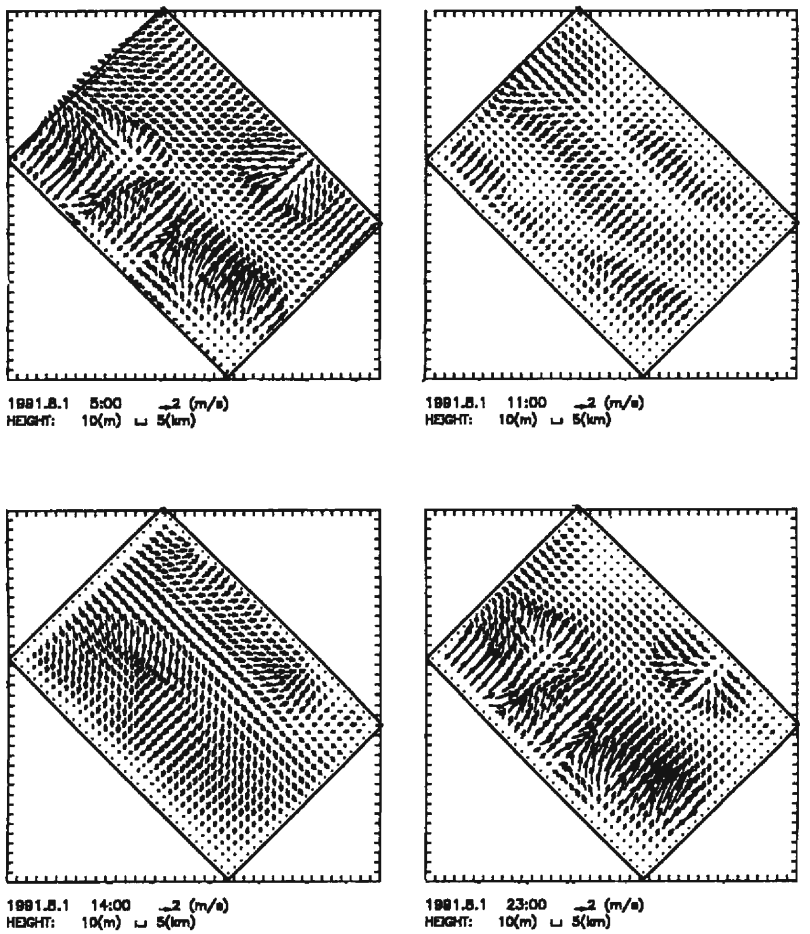

Fig. 6(a). Simulation results of local wind field at the level of 10 m above surface at 0500, 1100, 1400 and 2300 BST on August 1, 1991.

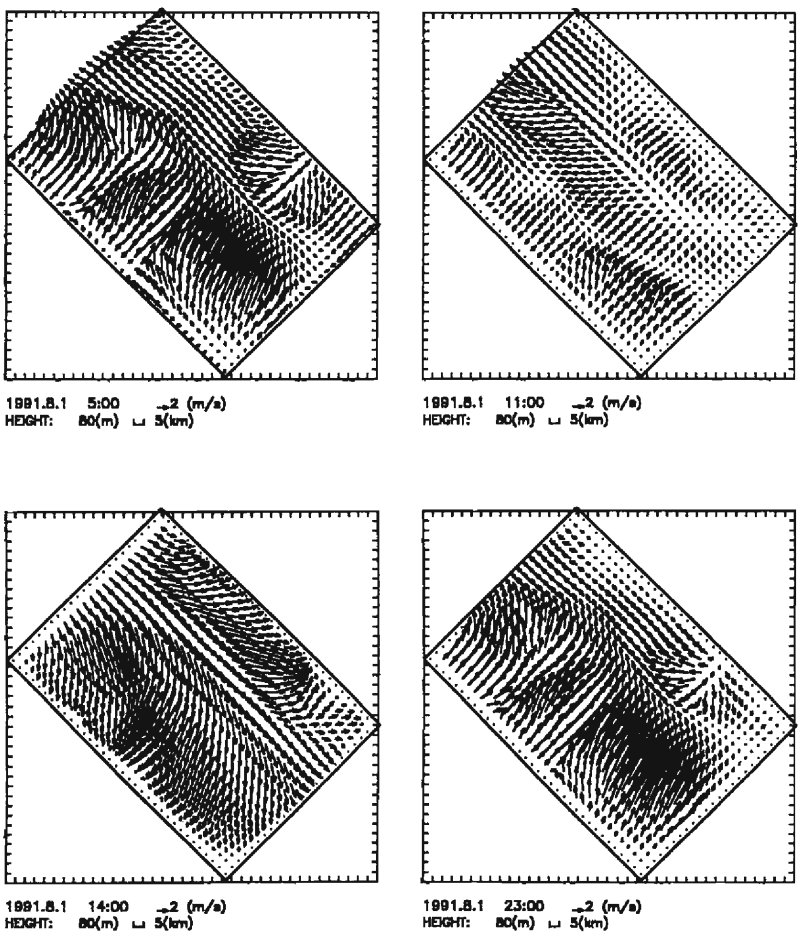

Fig. 6(b). Same as Fig. 6(a) but at the level of 80 m above surface.

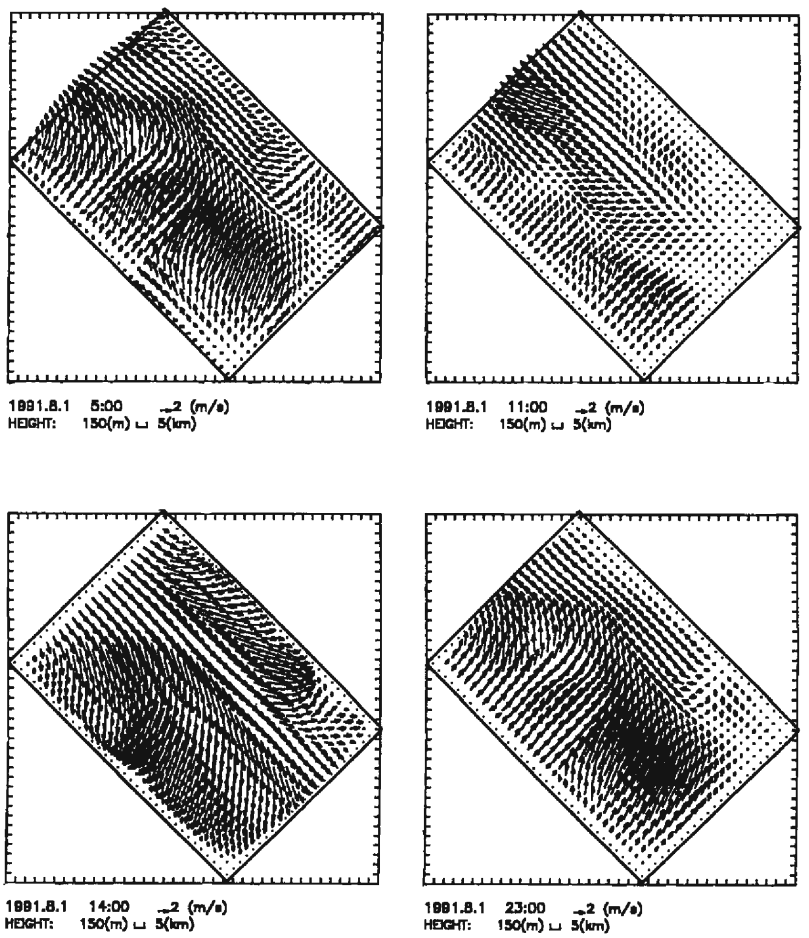

Fig. 6(c). Same as Fig. 6(a) but at the level of 150 m above surface.

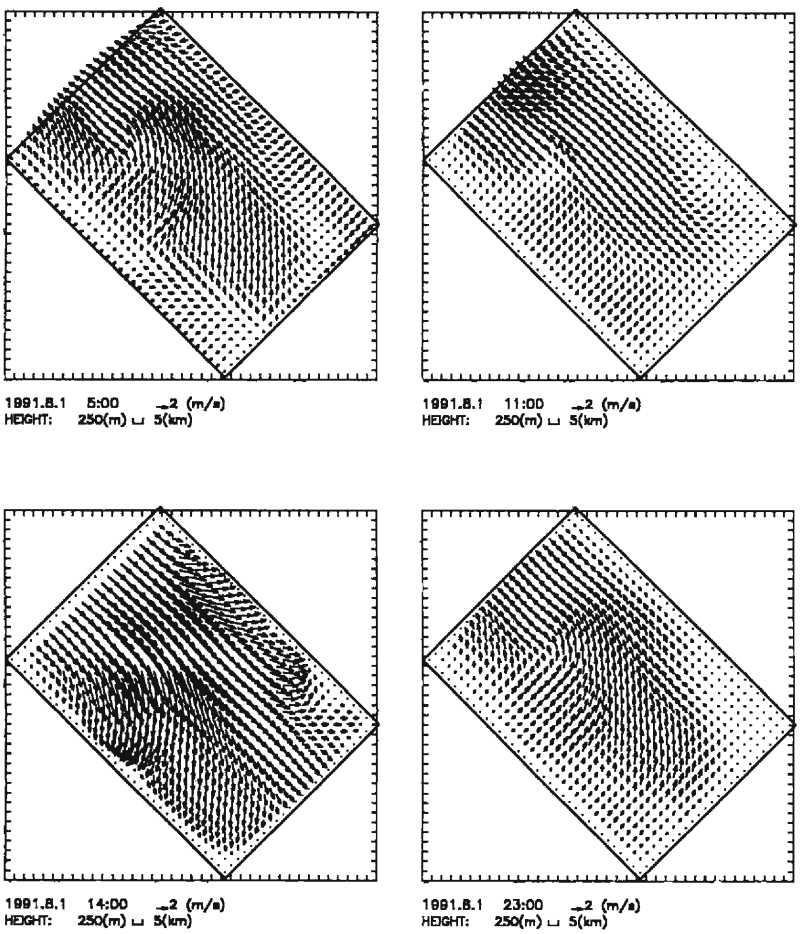

Fig. 6(d). Same as Fig. 6(a) but at the level of 250 m above surface.

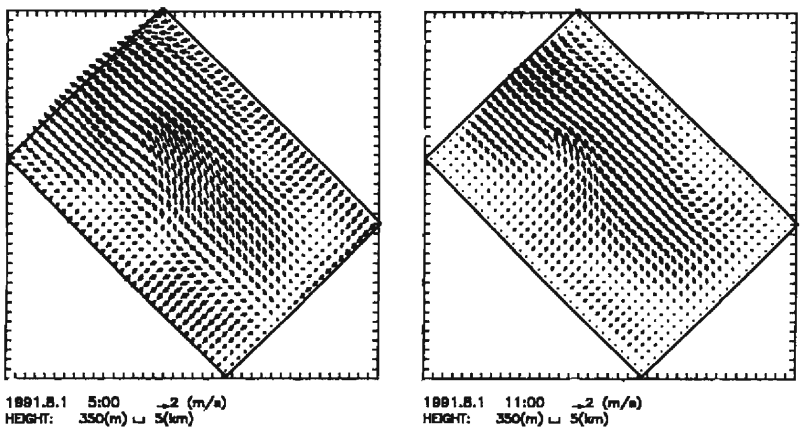

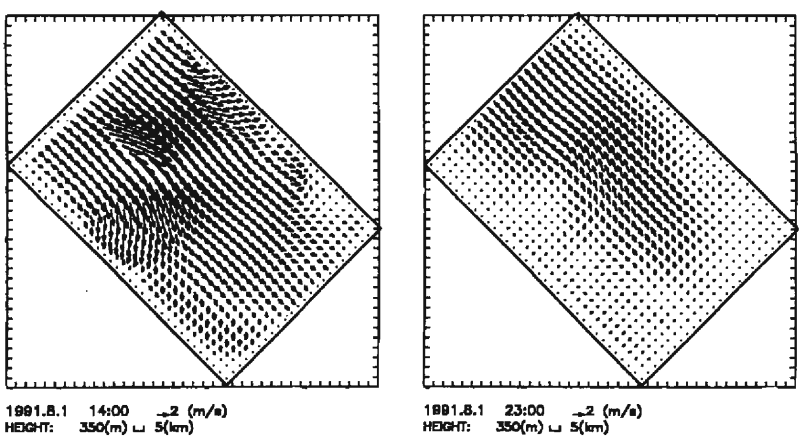

Fig. 6(e). Same as Fig. 6(a) but at the level of 350 m above surface.

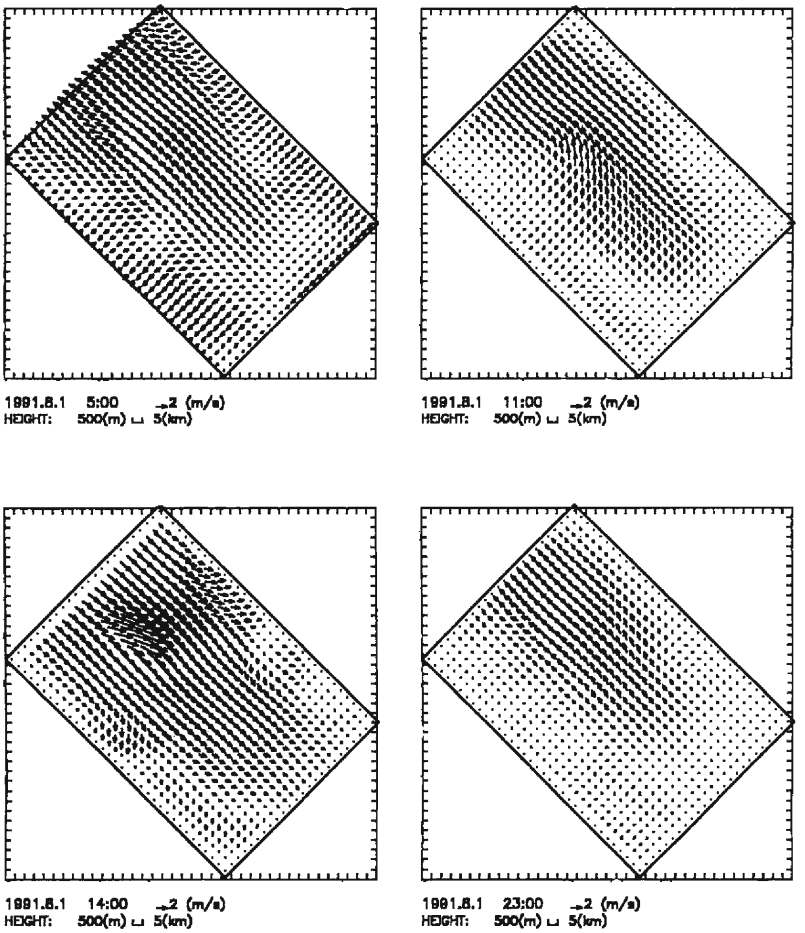

Fig. 6(f). Same as Fig. 6(a) but at the level of 500 m above surface.

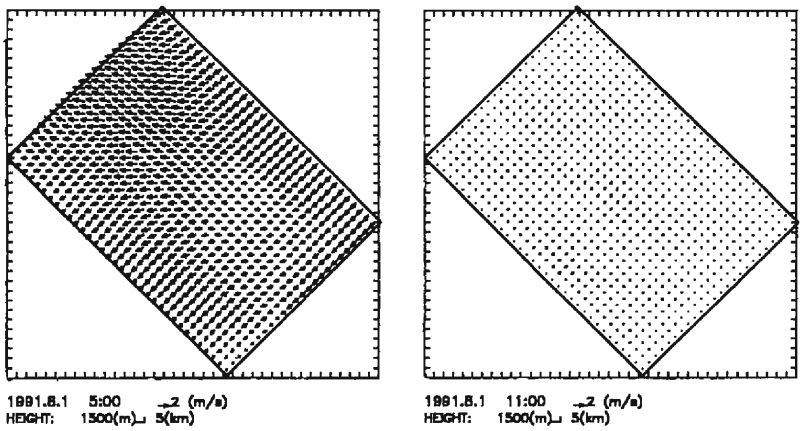

Fig. 6(g). Same as Fig. 6(a) but at the level of 1500 m above surface.

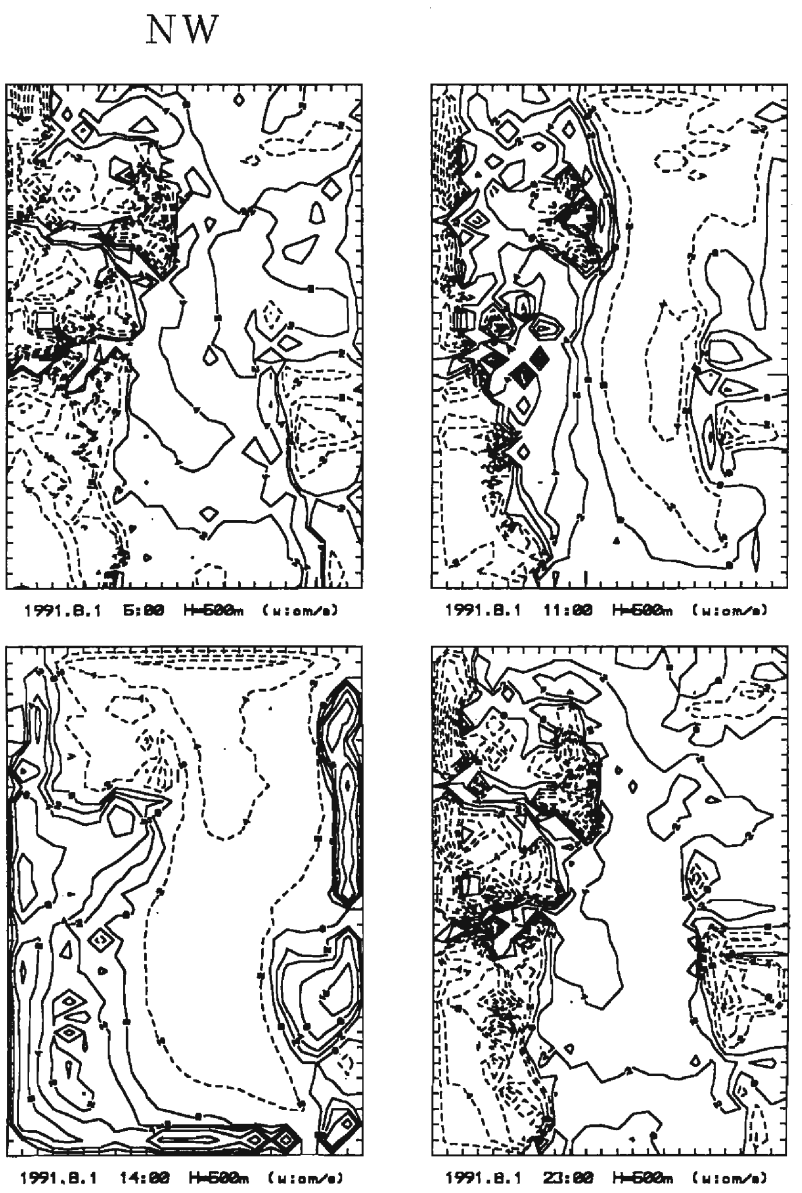

Fig. 7. Distribution of vertical velocity at the level of 500 m above surface. The solid line shows upward motion and the broken line downward motion.

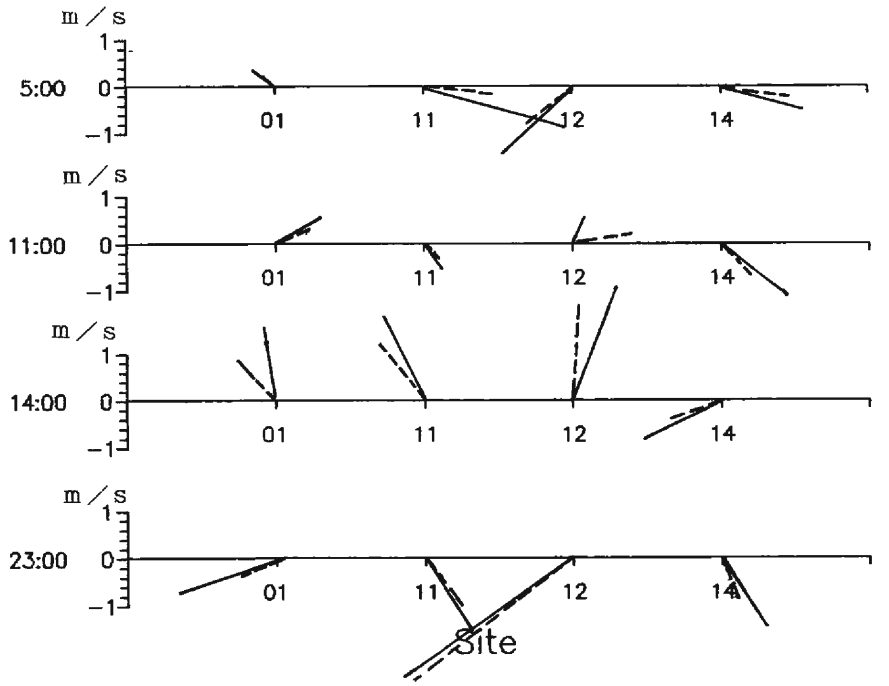

Fig. 8. Comparison of simulated and observed wind at some surface stations. The lines are the same as in Fig. 4.

Figs. 6(a) to 6(g), the vertical structure of these slope winds is revealed. The downslope wind from the Qilian Mountains is strong up to about 150 m above surface, but weakened at 250 m. The upslope wind to the Qilian Mountains is also strong at 150 m, and it continues up to about 350 m, whose height is a little higher than that of the downslope wind.

The wind which blows parallel to the Heihe river basin shows a different feature. The downvalley wind, southeasterly, is seen at 0500, 1100 and 2300 BST, and the upvalley wind, northwesterly, is seen at 1400 BST. The upvalley wind extended to the 500 m level at 1400 BST (Fig. 6(f)), and still remained northwest of the computational region at 1500 m in Fig. 6(g). The downvalley wind, southeasterly, is not as deep as the upvalley wind, but it exists at the 500 m level (Fig. 6(f)). Considering that the slope along the Heihe river basin is less steep than that of the mountains at both sides of the basin, it can be deduced that the upvalley and downvalley winds along the Heihe river basin may be partly fed by both upslope and downslope winds of both sides of the valley.

The distribution of the vertical wind component at 500 m is shown in Fig. 7. In the nighttime, 0500 and 2300 BST, the vertical component is upward over the basin but it is downward above the Qilian Mountains and LongShou Mountains. In the daytime, 1100 and 1400 BST, the sign of the vertical component is almost reversed. The downward component reaches −0.14 m/s near the Heishan Mountain, and the upward

component reaches 0.11 m/s near the YingLuoXia Valley.

The simulated surface wind is compared with the observed winds in Fig. 8. Noting the low wind condition in this case, the overall results of the simulation is fair, except that the model somewhat underestimates the wind velocity and there are larger deviations of the predicted wind direction from the observation at 1400 BST.

In general, the simulated field (Fig. 6) reproduced the basic features of the local circulation seen in the analyzed wind field (Fig. 5). (Note that the size of the analysis model is a little smaller than that of the simulation, but the grid size is the same). Further, it is noteworthy that the upslope/downslope winds over LongShou Mountain, which are not seen in the analyzed field, are well-simulated by the dynamic model. Although the MASCON is widely used as a model for wind field over complex terrain, it is basically an analysis model. Therefore, the model could not reproduce features peculiar to local circulation, unless these features be detected by the observation. We ran the MASCON with an additional artificial wind data at a site near LongShou Mountains. When the artificial data reflected the upslope/downslope components, the diagnostic wind field was quite similar to that of the dynamically simulated wind field. Thus, the numerical model helps us in understanding the meteorological field in the data sparse area.

5. Remarks

Three dimensional wind field in HEIFE experimental area was investigated using a numerical model based on the primitive equations with the parameterization of turbulence and surface processes. Two extreme cases, one for the strong synoptic wind and the other for thermally driven local circulation, were simulated. Although thorough verification of the performance of the model is difficult because of the insufficiency of the observation data, it can be said that the model successfully reproduced the basic features of observed wind fields in both cases. In the latter case the merit of the dynamic model was clearly demonstrated. The thermally driven local circulation greatly depends on such local features as surface condition and topography, for which the observation network was not enough to resolve the complexity of thermally driven local flow. Even though a sophisticated diagnostic model, MASCON, was used, it was impossible to reproduce such localized flow field. On the other hand, the dynamic model can reproduce highly localized flow. The other merit of dynamic model is that it can produce many quantities such as various kind of fluxes.

Acknowledgment

This contribution is a product of the HEIFE cooperative study project sponsored by Chinese National Nature Science Foundation and Japanese Ministry of Education, Science, Sports and Culture (Monbusho). The continuous support given by Peking University and Kyoto University are also appreciated. The first two authors express their appreciation to the Japanese Monbusho for arranging their visit to the Disaster

Prevention Research Institute, Kyoto University.

References

Arritt, R. W.: 1987, The effect of water surface temperature on lake breezes and thermal internal boundary layers, Boundary Layer Meteorol., 40, 101–125.

Blackadar, A. K.: 1962, 'The Vertical Distribution of Wind and Turbulent Exchange in a Neutral Atmosphere', *J. Geophys. Res.* 67, 3095–3102.

Chen, J., L. Pan, Y. Mitsuta, and K. Sahashi: 1993, A simple three dimensional flow model, International Symposium on HEIFE, 105–116.

Dickinson, R. E.: 1984, Modeling evapotranspuration for three dimensional global climate models, Climate processes and climate sensitivity, Geograph. Mongr., 29, 58–72.

Inoue, J. and Y. Mitsuta: 1990, Results and problems of test observation in the desert of HEIFE area. HEIFE Report No. 5, 165–221.

Jacquelyn, B. and J. Noilhan: 1990, Sensitivity study and validation of a land surface parameterization using HAPEX-MOBILTHY data set, Boundary-Layer meteorology, 52, 93–134.

Louis, J. F.: 1979, A parametric model of vertical eddy fluxes in the atmosphere, Boundary-Layer meteorology, 17, 187–202.

Noilhan, J. and S. Planton: 1989, A simple parameterization of land surface processes for meteorological models, Mon. Wea. Rev., 117, 536–549.

Pielke, R. A.: 1984, Mesoscale meteorological modeling, Academic Press, New York, N.Y.

Sahashi, K., O. Tsukamoto, Y. Mitsuta, and J. Chen: 1993, Features of wind field at the desert station and the oasis station, International Symposium on HEIFE, 396–401.

Sang, J., Y. D. Wu, H. Zh. Liu, N. X. Pan, J. Y. Chen, and H. Ch. Zhang: 1992, The simulation of atmospheric boundary layer over non-uniform surface, Plateau Meteorology, 11, No. 4, 400–409.

Tang, M. C.: 1963, The climatic diurnal variation over Qi Lian mountain, Geophysical Journal, Vol. 29, No. 3, 197–206.

Yamada, T.: 1983, Simulation of nocturnal drainage flow by a q^2-l turbulence closure model. J. Atmos. Sci., 40, 91–106.